NON-LINEAR MODELING OF FLAT-PLATE SYSTEMS UNDER CYCLIC LOADING

S. Derogar & C. Ince
Yeditepe University, Turkey

P. Mandal
University of Manchester, UK

Y. C. Toklu
Bayburt University, Turkey

SUMMARY:
There are two methods to model the lateral load response of slab-column frames; Effective Beam Width Method (EBWM) (Han *et al.* 2009) and Equivalent Frame Model (EFM) (Park *et al.* 2009,). Different researchers calibrate their model derived from experiments using one of these two methods. Also, current design codes (ACI 318-08, Eurocode 2-2004) permit the EFM for the analysis of two-way slab systems under gravity loads, as well as lateral loads such as seismic loads. This study shows that both the "EBWM" and "EFM" models are not appropriate in accurately predicting the response of slab-column frame systems under lateral loads. An artificial neural network limit state model for the drift ratio is developed for the first time to the analysis of slab-column connections under cyclic loading.

Keywords: Slab-column connection, punching shear failure, Artificial Neural Network, analytical modelling.

1. INTRODUCTION

Equivalent frame model (EFM) and the effective beam width model (EBWM) are often used to analyze the flat slab structures. EBWM is useful in modeling the flat slabs under lateral loads where the flat slab is actually modeled as an effective beam having the same depth as the slab and an effective beam width (effective width factor×slab width). Propagation of further cracks in the slabs is observed as the level of applied moments due to later loads increased. Hence, the analysis of flat slab structures should take the reduction in slab stiffness into account as this is entirely due to the effect of cracks. Different suggested stiffness reduction factor can be found in the literature (Hwang and Moehle, 2000; Luo and Durrani, 1994). However, using a recommended constant stiffness reduction factor (e.g. β=1/3, recommended by Vanderbilt and Corley, 1983) results in overestimating the lateral drifts and slab moments of the structure. Hence, the overall aim is to develop a robust model capable of incorporating important response features of slab column connections. In this paper, a limit state model, initially developed by Elwood (2003), further adopted by Kang (2004), is used to model the punching shear of slab column connection. For this purpose, an artificial neural network limit state model is developed for the first time to predict the drift ratio at punching failure. Slabs (referred here as slab S1 and S4) from experiments reported by Derogar *et al.*, 2007 are adopted to use in the analytical modeling.

This paper also aims to assess the lateral stiffness of the slab-column connection using effective beams width model. This is achieved by applying the α, β values available in the literature (Pecknold, 1975; Allen *et al.*, 1977; FEMA 274 and ASCE/SEI 41) to the slab-column connection model. Suggested values of α, β are used to calculate the bending stiffness of the "slab" beams in the analytical non-linear model. The experiments reported by Derogar *et al.*, 2007are used to compare to the analytical results in this paper. The modeled slab configuration and the modeled slab test setup are shown in Fig. 1.1 (a) and (b) respectively.

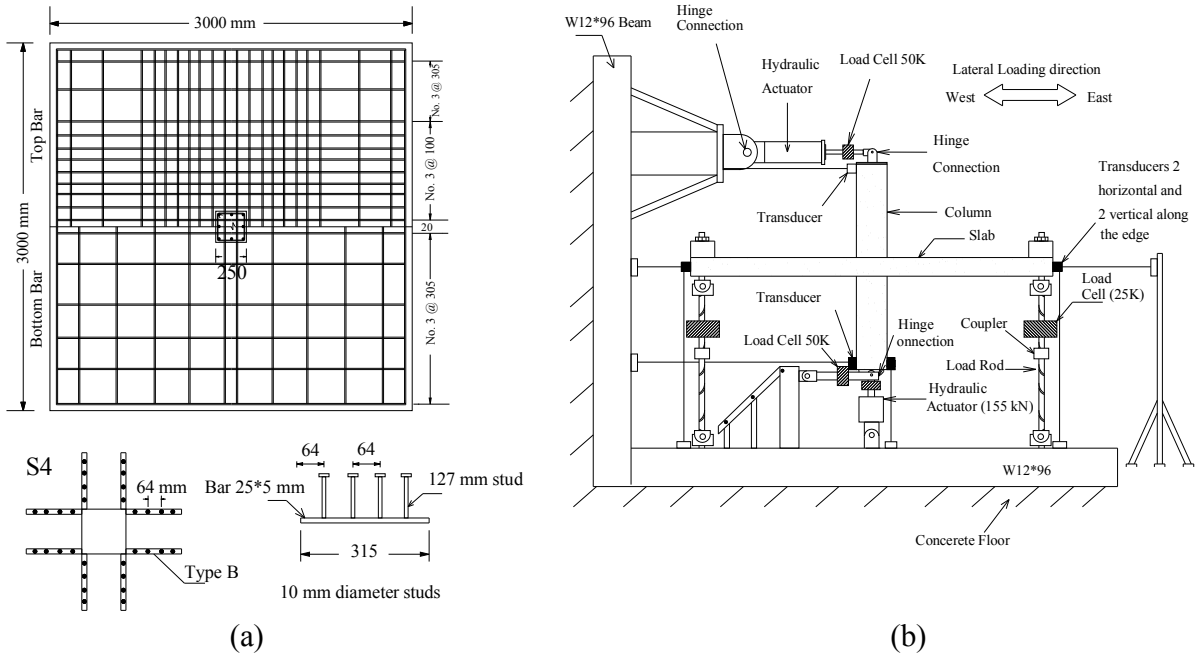

Figure 1.1 The Modelled slab configuration (b) The modelled slab test setup (Derogar *et al*. 2007)

2. LATERAL-LOAD STIFNESS USING EFFECTIVE SLABWIDTH MODEL

An analytical model for test specimen S2 was created to compare the response from analytical model with response obtained during the test. Response of test specimen for approximately the first 10 cycles was effectively within the elastic range of the test specimen. For this reason, the first 10 cycles of the response was compared with the analytical model to determine appropriate α- and β-factors for the effective slab width model. The structure was modeled using the OpenSees platform (2007) as a plane frame as shown in Fig. 2.1.

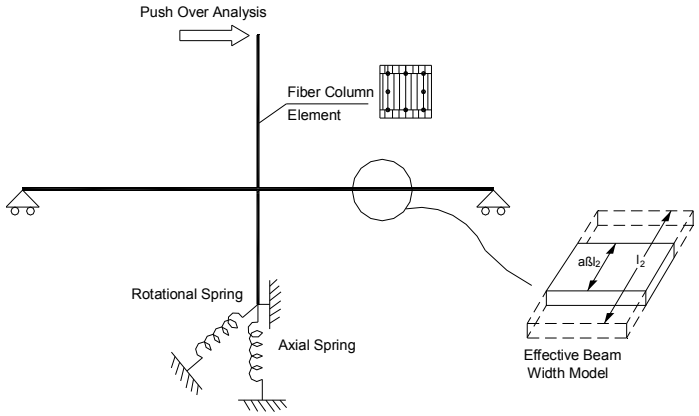

Figure 2.1 Plane frame modelling of the test structure

A fiber model, with the material properties based on results obtained in material testing, was used for the column. Axial and rotational springs were included in the model at the base of column to account for the gravity load. The slab-column joint was assumed to be rigid and the use of this assumption tends to correlation with test results as indicated in related studies. Table 2.1 shows the recommended values for α and β factors from Pecknold, 1975; Allen *et al*., 1977; ASCE/SEI 41; and FEMA 274. ASCE/SEI 41 uses the recommended values of α and β from Hwang *et al*., 2000.

Table 2.1. The recommended values of α and β form different models

Models in the Literature	α values	β values
Pecknold (1975)	0.7	0.68
Allen et al. (1977)	0.54	0.557
FEMA 274	0.5	0.333
ASCE/SEI 41	0.5	0.333

Pushover analyses were conducted using different α and β values in the analytical model (shown in Table 2.1) in order to compare with the experimental result. Results presented in Fig. 2.2 indicate that the values obtained from FEMA 274 or ASCE/SEI 41 for α and β capture the lateral load versus displacement response of the tested system reasonably well. It can be concluded that the recommended values from FEMA 274 correlate well with the experimental results. Therefore, the suggested values of α and β by FEME 274 are used in the modeling of slab beam element in the next section.

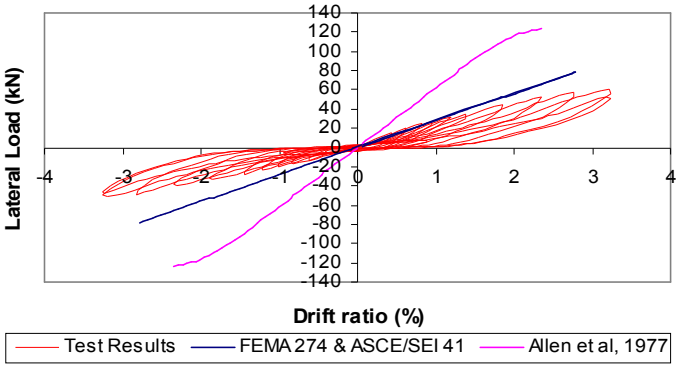

Figure 2.2 Lateral load Verse Drift Ratio (%) for specimen S2

3. ANALYTICAL MODEL

Modelling the behaviour of slab-column frame is complicated by the need to address the potential for punching failures at slab-column connections, which may occur by either stress-induced failure or drift-induced failure. Stress-induced failure refers to the case when the shear stress on the slab critical section exceeds the nominal shear stress and drift-induced failure refers to the case when the shear capacity degrades to the point where it equals the demand. (Pan *et al*., 1989; and Kang, 2004). Shear demand-capacity relation by Aschheim *et al*., 1992 is shown in Fig. 4.1. Moehle in 1996 reported that punching failure of slab-column connection is primarily a function of gravity shear ratio on the slab column critical section and the interstory drift ratio imposed on the connection. Additional factors that can affect the modeling of the slab-column behavior are the connection type (interior, exterior, and corner), and whether the shear reinforcement is provided. This section is focused on modeling the behavior of interior slab-column connections with and without shear reinforcement.

4. MODELING

The three-dimensional interior slab-column connections tested under reversed cyclic loading were modeled as plane frames as shown in Fig. 4.2. A fiber model (Spacone *et al*., 1996) was used for the column. The column fiber model developed by Spacone *et al*., 1996 is relatively simple model which accurately captures nonlinear flexural-axial load behavior. The column cross section was subdivided into confined (core) and unconfined (cover) concrete fibers, and steel (rebar) fibers. The slab-column joint was assumed to be rigid, as studies indicate that use of this assumption tends to produce better results (Allen *et al*,. 1977). The α and β values used for the "slab" beam element in the analytical model were 0.50 and 0.33 respectively as discussed in section 2. The OpenSees platform (2007)

(version 2.0) is used to conduct the analytical studies. The following subsections describe the plane frame model and the models for each component.

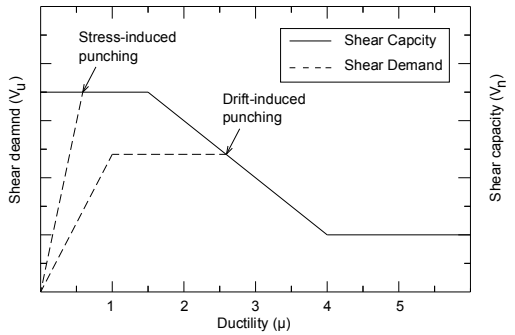

Figure 4.1 Shear demand-capacity relation (Aschheim *et al*., 1992).

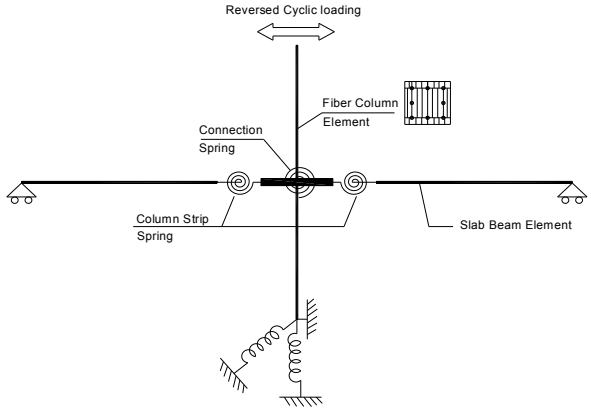

Figure 4.2 Plane frame modelling

4.1 Slab-column connection modelling

The nonlinear behavior due to yielding of slab reinforcement within the column strip or within the slab transfer width of $c_2 + 3h$ adjacent to the slab-column connections is modeled as shown in Fig. 4.3. A rigid-plastic connection (torsional) spring is used to monitor the moment transfer at the slab-column connection. Column strip springs monitor slab moments on either side of the slab-column connection. Nonlinear slab responses are modeled using zero length plastic hinges at the end of the slab-beam. Nonlinear behavior of the slab-column connection is modeled using a rigid-plastic connection spring in combination with the limit state model. Linear and nonlinear column responses are modeled using a fibres model, as described earlier. Given this model, flexural yielding occurs only if the nominal moment capacity of the column strips plastic hinge is reached, or if the unbalanced nominal moment capacity of the connection spring (i.e., rigid-plastic torsional spring) is reached. Punching failure is monitored using the rigid-plastic connection spring, and can occur if the shear stress on the slab critical section reaches a critical value (stress-induced failure) (as defined in ACI 318-08, Equations 11-33 to 36), or if the limit state associated with interstory drift versus gravity shear stress ratio on the slab critical section is reached (drift-induced failure).

4.2. Punching failure prior to yielding of slab reinforcement

Punching failure prior to yielding of slab reinforcement occurs when the sum of direct gravity shear stress and shear stress induced by the fraction of unbalanced moment transferred by eccentric shear reaches the shear stress capacity on the slab critical section as shown in case (a) in Fig.4.3.

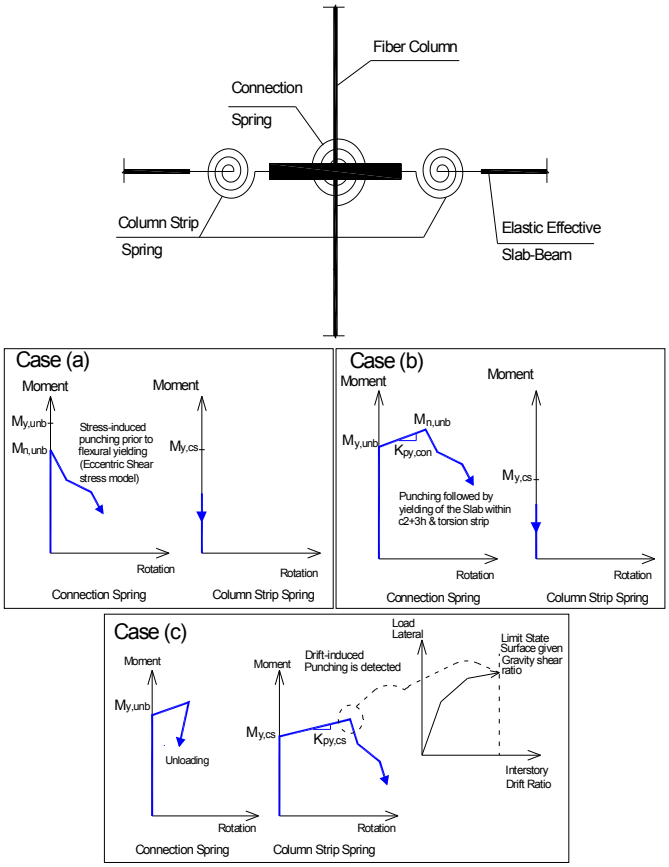

Figure 4.3 Modeling of slab-column connection (adopted from Kang, 2004)

$$v_u = \frac{V_g}{b_o d} \pm \frac{\gamma_v M_{u,unb} c}{J_c} = v_n \tag{4.1}$$

where b_0=the perimeter of critical section, d = the effective slab depth, γ_v = the fraction of unbalanced moment transferred by eccentric shear, $M_{n,unb}$ = the unbalanced moment, c is the distance from the centroid of the critical section to the perimeter of the critical section that results in the smallest value of $M_{n,unb}$, J_c = property of assumed critical section analogous to polar moment of inertia, and v_n = nominal shear stress capacity at the connection. The nominal shear strength on the critical section within the shear reinforced region is $v_n = v_c + v_s$, whereas the nominal shear strength for the critical section outside the shear reinforced zone is $v_n = v_c$, where v_c and v_s are the nominal shear stress capacities provided by the concrete and the shear reinforcement, respectively. Once the shear strength is reached, the strength of the connection spring ($M_{n,unb}$) drops suddenly.

4.3 Yielding of slab reinforcement followed by punching failure

Fig. 4.3 (b) shows the rigid-plastic connection spring model for the case yielding of slab reinforcement occurs prior to punching failure. The yield capacity for connection spring ($M_{y,unb}$ in Fig. 4.3) is computed based on the slab reinforcement provided within the transfer width of $c_2 + 3h$ as this transfer width for FEMA 356 and is $c_2 + 5h$.

$$\gamma_f M_{y,unb} = \left(M^{+}_{y,c_2+3h} + M^{-}_{y,c_2+3h}\right) \quad (4.2)$$

Where $M^{+}_{y,c+3h}$ $(or\ M^{-}_{y,c+3h})$ is the yield moment of the slabs framing into a connection over a transfer width for positive bending (or negative bending).Since only a fraction of the unbalanced moment is assigned to flexure (e.g., $\gamma_f M_{y,unb}$), the remaining portion of the unbalanced moment ($\gamma_v M_{y,unb}$), assigned to eccentric shear, is less than that required to result in punching failure using the eccentric shear stress model (i.e., slab yielding occurs prior to punching failure). Fig. 4.3 (c) shows that after yielding of the connection spring, additional moment transfer at the slab-column connection is possible because additional capacity beyond $M_{y,unb}$ exists to transfer moment by eccentric shear (since punching failure has not occurred); therefore, additional moment is transferred only by eccentric shear (i.e., $\gamma_f = 0\ and\ \gamma_v = 1$ after reaching M_{n,c_2+3h}). Post-yield stiffness ($K_{py,conn}$) defined by the additional unbalanced moment that results in yielding within the column strip, divided by the plastic rotation ($\theta_{pl,conn}$) over a transfer width of $c_2 + 3h$. Kang (2004) showed that $\theta_{pl,conn}$ could be approximated as $(3/2)(\phi_{y,c+3h})(h)$, where $\phi_{y,c+3h}$ is the yield curvature of the slab over the width of c2+3h. Parametric analytical studies carried out by Kang (2004) indicated that use of $K_{py,conn}$ equal to 100% of the elastic stiffness of the slab (EI cracked) for an interior connection, produced approximately equivalent results of using a post-yield stiffness derived using the yield curvature, indicating that the model results are not overly sensitive to the value of $K_{py,conn}$.

4.4. Punching failure after flexural yielding within the column strip

Flexural yielding within the slab adjacent to the slab-column connection is considered on either side of an interior connection when using column strip (rotational) springs as shown in Fig. 4.3 (c). Punching failure is modeled by assuming that the moment capacity of the slab drops to a (zero) residual capacity once a critical story drift ratio is reached. The critical story drift ratio is detected by using a limit state model (Elwood, 2004), as discussed subsequently. The yield moment capacity of the column strip spring ($M_{y,cs}$) is modeled separately from the nominal moment capacity of the connection spring ($M_{u,unb}$), such that punching failure can result from either reaching a limiting story drift for a given gravity shear ratio (reaching the limit state) or reaching the capacity of the connection spring (eccentric shear failure). The estimated post-yield stiffness for the column strip springs ($K_{py,cs}$) ranged between 10 to 20% of the elastic (cracked) stiffness of the slab for the test structures (Kang, 2004); therefore, an average value of 15% of the elastic stiffness can be used for all connections. Alternatively, $M_{y,cs}$ may be estimated as $M_{n,cs}$ and the post-yield stiffness can be assigned a value close to zero, where $M_{n,cs}$ is the nominal moment strength of the slabs over the column strip. Values for the yield and nominal capacities, and the post-yield stiffness values for all springs are summarized in Table 4.1.

Table 4.1. Modeling of connection and column strip springs

RC	Spring Type	Yield Capacity	Nominal Capacity	Post-yield Stiffness
Interior Connection	Connection Spring ($\gamma_f = 0.75$)	$M_{y,unb}\,[kN-m]$	$M_{n,unb}\,[kN-m]$	$K_{py,con}\,[kN-m/rad]$
		+81.85	+93.5	1305
		-81.85	-93.5	1305
	Column Strip Spring	$M_{y,cs}\,[kN-m]$	$M_{n,cs}\,[kN-m]$	$K_{py,cs}\,[kN-m/rad]$
		+24.0	+31.0	110
		-67.00	-74.0	270

4.5. Limit State Models

Elwood *et al*., (2002) developed a limit state model which can be defined by using nominal shear strength versus interstory drift (e.g., Elwood, 2004), whereas for slab-column connections, the limit state surface can be defined using the gravity shear stress ratio versus interstory drift (Robertson *et al*., 2002 and Kang, 2004). Once the limit state surface is reached (i.e., a prescribed drift limit is reached for a given gravity shear ratio), a punching failure is "detected" and the ability of the slab-column connection to transfer moment (or unbalanced moment) degrades according to a specified relationship. The limit state model for slabs developed by Kang (2004) was based on the best fit line by applying linear regression analysis on a limited collected test data (40 experiments) on slabs without shear reinforcement. Therefore, this can lead to overestimate or underestimate of the rotation capacity of the slab column connections in the model. In this work a limit state model for drift capacity based on Artificial Neural Network which was developed by Derogar and Mandal (2012) is adopted.

5. ANN MODEL FOR DRIFT RATIO- LIMIT STATE MODEL

5.1 Artificial Neural Network

Artificial Neural Network is a mathematical model or computational model that tries to simulate the structure and/or functional aspects of biological neural networks. It is made up of a large number of simple processing units known as neurons (or nodes or units) which are connected to each other to form a network (Iruansi, 2012). The connections have weights associated with them referred to as synaptic weights. Each signal travelling along a connection is multiplied by the its weight. In developing an artificial neural network eight parameters; concrete cylinder strength, percentage of flexural reinforcement, yield stress of flexural reinforcement, span length, effective depth, column shape, column dimension, and percentage of compression reinforcement were chosen for slabs without shear reinforcement and thirteen parameters; concrete cylinder strength, percentage of flexural reinforcement, yield stress of flexural reinforcement, span length, effective depth, column shape, column dimension, and percentage of compression reinforcement, yield stress of shear reinforcement, area of shear reinforcement in 0.5d, 1.0 d, 1.5d and 2.0 d from the column perimeter were chosen for slabs with shear reinforcement as shown in Fig. 5.1. For modeling purposes a feed-forward neural network using a back-propagation algorithm was employed. The optimum number of hidden layers, the number of processing elements and the network parameters used, are achieved by trial and error process. Thus a hidden layer with 5 neurons and 7 neurons were used for slabs without and with shear reinforcement respectively in this study. Fig. 5.1 (a) and (b) show the architecture of typical neural networks for slabs without and with shear reinforcement respectively. Full detail of the ANN model is discussed in Derogar and Mandal 2012.

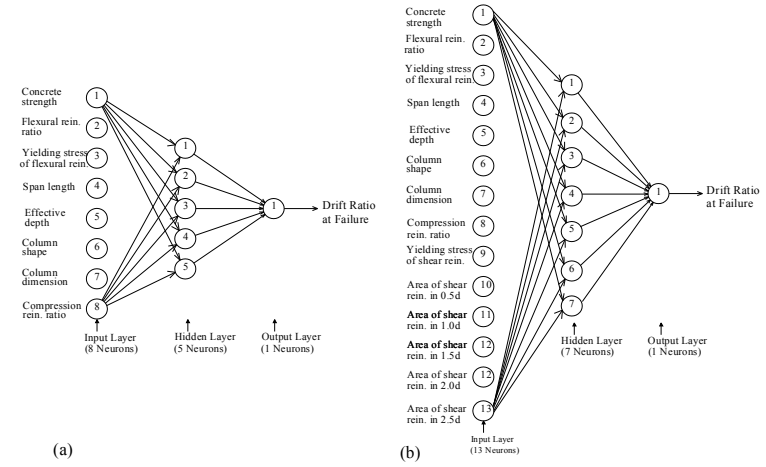

Figure 5.1 Architecture of selected network: (a) slabs without shear reinforcement (one hidden layer with five neurons) (b) Slabs with shear reinforcement (one hidden layer with seven neurons)- for clarity, not all neuron connections are shown.

Computations were done by programming in Matlab, using function “newff” which creates a feed forward network. Tan sigmoid transfer function was used as shown in Fig. 5.2.

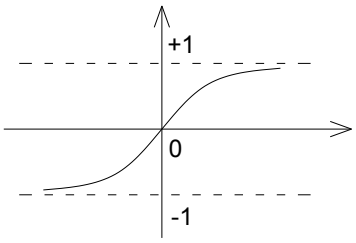

Figure 5.2 Tan-Sigmoid Transfer Function

The ANN shown in Fig. 5.2 can be explained as below: The error, E, between the computed value (denoted by O_K) and the target output (denoted by T_K) of the output layer is defined as

$$E = \frac{1}{2}\sum_{K=1}^{n}(O_K - T_K)^2 \tag{5.1}$$

$$O_K = F(I_i W_i^K) = F\left(\sum_{i=1}^{3} I_i W_i^K\right) \tag{5.2}$$

In the above equation, $F(...)$ is the tan sigmoid function, I_i is the input to neuron "K" of the single output layer from the neuron i of the hidden layer, and W_i^K is the weight associated between neuron i of the hidden layer and neuron "K" of the output layer (Mansour *et al.* 2004). 52 experiments on slabs without shear reinforcement and 35 experiments on slabs with shear reinforcement were used in the development of ANN model. This database is adopted from Derogar and Mandal, 2012. Fig. 5.3 (a) and (b) shows the drift ratio of the slabs at failure, predicted by ANN models for slabs without and with shear reinforcement. It is clear from the figure that ANN is able to predict the drift ratios at failure with very high accuracy compared to the best fit line model developed by Kang 2004.

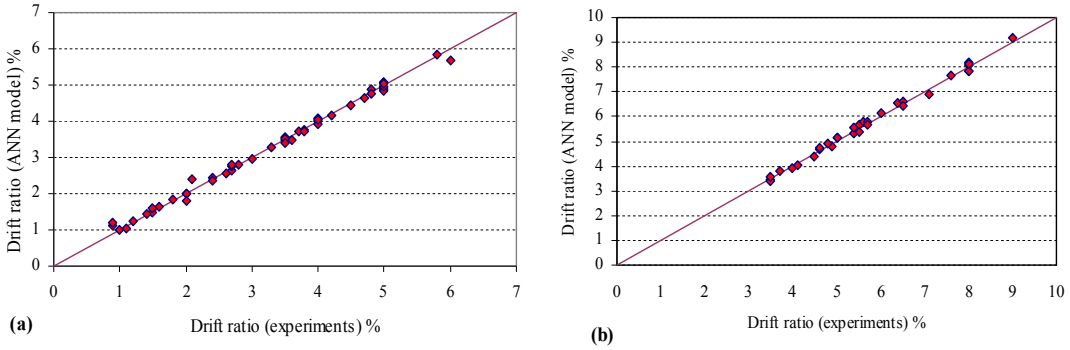

Figure 5.3 Comparison between measured and ANN predicted drift ratios at failure for (a) slabs without shear reinforcement (b) slabs with shear reinforcement.

5.2. Post-punching behaviour and hysteretic behaviour

When the story drift ratio reaches the limit state surface, the strength and stiffness (K_{deg}) degrade as shown for Fig. 4.3 (c). The slopes (stiffness values) of both the connection and column strip springs

assigned after reaching the limit state are set to relatively small values for the cyclic reversed loading test specimens (e.g., 5% of the nearly infinite elastic stiffness of the springs; 225 kN-m/rad (RC) to avoid numerical convergence problems (i.e. an infinite slope cannot be used)). The existing hysteretic model available in OpenSees (Elwood *et al*., 2003) was used to capture the hysteretic behavior (slab and slab-column connection). The model used includes the following parameters: p_x is a pinching factor for deformation during reloading, p_y is a pinching factor of force during reloading, and $\mu^{-\beta}$, where μ is the displacement ductility and β is a parameter to define the unloading stiffness (Elwood *et al*., 2003). Theoretically, parameters p_x, p_y, and β can vary between zero and one; however, for this analysis, values of p_x *and* p_y of 0.5 and 0.2, respectively, and β of 0.5 were used.

6. NONLINEAR STATIC REVERSED CYCLIC LOADING ANALYSES

Static reversed cyclic loading analyses were conducted to compare model results with envelop results measured during the cyclic loading tests for the specimens S1 and S4. Gravity load tributary to the column strip was applied to the column via an axial spring. This axial spring was assumed to take a very small deformation. The experimental results for specimen S1 and S4 are shown in Figures 10 and 11 and are compared to the analytical studies. It can be seen that experimental results are in a very good agreement with analytical results and this indicates that analytical model is predicting the punching failure very well. According to the results from specimen S1, yielding top bars occur only within $c_2 + 3h$ width, which is consistent with the result obtained in the analytical model. Fig. 6.1 and Fig. 6.2 compares the results from the analytical model to the experimental results for specimen S4. In specimen S4 yielding of the slab flexural reinforcement is observed on both $c_2 + 3h$ and column strip Fig. 4.3 (c).

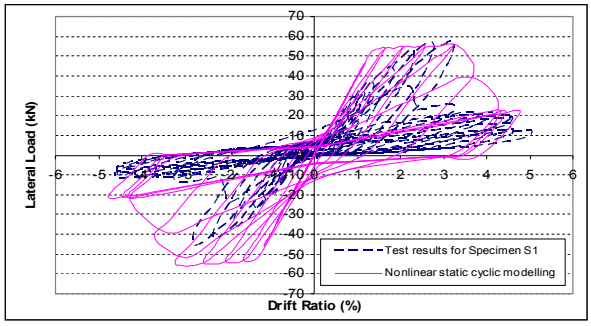

Figure 6.1 Lateral loads versus drift ratio for Specimen S1

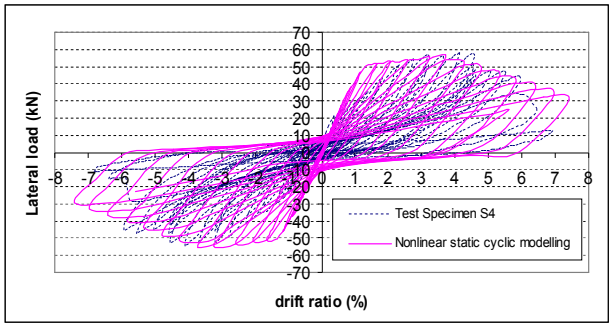

Figure 6.2 Lateral load versus drift ratio for Specimen S4

7. CONCLUSION

Analytical studies were conducted to assess appropriate modification factors to use for effective slab width (α) and cracking (β) for lateral load analysis of slab-column frames. Using an effective slab width model and a column fiber model, α-values of 0.50, and β-values of 1/3, resulted in generally good correspondence between experimental and analytical results and are similar to the values suggested in FEMA-274 (1997). In this paper, also a non-linear model for the slab-column connections subjected to gravity loads combined with lateral reversed cyclic forces was developed. An ANN limit state model for drift ratio was developed for the first time. The limit state model shows an excellent agreement with the experiments when compared to the other models available in the literature.

REFERENCES

ACI-ASCE Committee 421, (1999), Shear Reinforcement for Slabs (ACI 421.1R-99). American 24 Cconcrete Institute, Farmington Hills, Mich.

Allen, F. H., and P. Lep. Darvall, (1977), Lateral Load Equivalent Frame. ACI Structural Journal, Proceedings 74: 7, pp. 294-299.

ASCE/SEI 41, (2007). Seismic Rehabilitation of Existing Buildings. American Society of Civil Engineers, Reston, VA.

Aschheim M., Moehle J. P. (1992). Shear Strength and Deformability of RC Bridge Columns Subjected to Inelastic Cyclic Displacement. Earthquake Engineering Research Center, Report No. UCB/EERC-92/04.

Derogar, S., Guadagnini, M., Pilakoutas, K. (2007), Cyclic Testing of Slab-Column Connections with Lenton Fortress Steel Reinforcement. In Concrete Communication Symposium, Sheffield, UK.

Derogar S., Mandal P. (2012). Development of Artificial Neural Network for predicting the drift ratio at punching shear failure. To be submitted to Structural Engineering.

Elwood, K. J. (2002). "Shake Table Tests and Analytical Studies on the Gravity Load Collapse of Reinforced Concrete Frames," PhD Thesis, Department of Civil and Environmental Engineering, University of California at Berkeley, CA.

Elwood K. J., Moehle J. P. (2003). Shake Table Tests and Analytical Studies on the Gravity Load Collapse of Reinforced Concrete Frames. PEER Report 2003/01, Pacific Earthquake Engineering Research Center, University of California, Berkeley.

Elwood, K. J. (2004). Modelling failures in existing reinforced concrete columns. Canadian Journal of Civil Engineers, 31: 846–859, doi: 10.1139/L04-040.

FEMA 274. (1997), EHRP Commentary on the Guidelines for Seismic Rehabilitation of Buildings. FEMA Publication No. 274, prepared by the Building Seismic Safety Council for the Federal Emergency Management Agency, Washington, D.C.

FEMA 356, (2000). Prestandard and Comment for the Seismic Rehabilation of Buildings. FEMA Publication No. 356, prepared by the American Society of Civil Engineers for the Federal Emergency Management Agency, Washington, D.C.

Eurocode 2: Design of Concrete Structures- Part 1-1: General rules and rules for buildings, BS EN 1992-1-1:2004.

Hwang, S. J., and Moehle, J. P. (2000). Vertical and Lateral Load Tests of Nine-Panel Flat-Plate Frame. ACI Structural Journal, 97: 1, Jan.-Feb., pp. 193-203.

Iruansi O. (2012). Towards the Understanding of NonLinear Behaviour of Reinforced Concrete Members Failing in Shear, The University of Sheffield, PhD thesis.

Kang T. H. K., (2004). Shake Table Tests and Analytical Studies of Reinforced and Post-tensioned Concrete Flat Plate Frames. University of California, PhD Thesis.

Han S.W., Park Y.M., Kee S.H., (2009). Stiffness Reduction Factor for Flat Slab Structures under Lateral Loads. Structural Engineering. 135: 6, June 1, 2009. ©ASCE, ISSN 0733-9445/2009.

Luo, Y. H., Durrani, A. J., Conte J. P., (1994). Equivalent Frame Analysis of Flat Plate Building for Seismic Loading. Journal of Structural Engineering, ASCE. 120: 7, pp. 2137-2155.

Mansour , M.Y., Dicleli, M., Lee, J.Y., and Zhang, J. (2004). Predicting the shear strength of reinforced concrete beams using artificial neural networks. Engineering Structures. 26, pp. 781-799.

Moehle, J. P. (1996). Seismic design considerations for flat-plate construction. ACI SP-162: Mete A. Sozen Symposium, Farmington Hills.

OpenSees Development Team (2007). OpenSees: Open System for Earthquake Engineering Simulations," Version 1.5, Berkeley, CA.

Pan, A. D., and Moehle, J. P. (1989). Lateral Displacement Ductility of Reinforced Concrete Flat Plates. ACI Structural Journal. 86: 3, May-June, pp. 250-258.

Park Y.M., Han W.W., Kee S.H. (2009). A modified equivalent frame method for lateral load analysis. Magazine of Concrete Research. 61: 5, June, 359–370, doi: 10.1680/macr.2008.00081.

Pecknold, D. A. (1975). Slab Effective Width for Equivalent Frame Analysis. ACI Structural Journal. 72: 4, pp. 135-137.

Robertson, I. N., Kawai, T., Lee, J., and B. Enomoto (2002). Cyclic Testing of Slab-Column Connections with Shear Reinforcement. ACI Structural Journal, 99:5, pp. 605-613.

Spacone, E., Filippou, F. C., and Taucer, F. F. (1996). Fiber Beam-Column Model for Nonlinear Analysis of R/C Frames: Part I. Formulation: Earthquake Engineering and Structural Dynamics. 25, pp. 711-725.

Vanderbilt, M. D., Corley W. G. (1983). Frame Analysis of Concrete Building. Concrete International: Design and Construction. 5:12, pp. 33-43.